PAPER

Nitron-derivative-based palladium carbene complexes: structural characterization, theoretical calculations, and catalytic applications in the Mizoroki–Heck coupling reaction†

Ming-Yi Lee, Chih-Hsiang Liao, Hsiu-Yu Hung, [ID] Jhen-Yi Lee* and Hon Man Lee [ID] *

New palladium(0) and palladium(II) complexes with *N*-heterocyclic carbene (NHC) ligands derived from nitron and its derivatives were synthesized. The structures of most of these complexes were established by single-crystal X-ray diffraction studies. Among the new complexes, the palladium complex with a monodentate NHC ligand derived from nitron demonstrated the highest efficacy as a catalyst precursor in the Mizoroki–Heck coupling reaction of aryl chlorides with alkenes. Theoretical calculations provide valuable insights into the electronic parameters of both the ligands and the palladium complexes, highlighting the significance of a robust Pd–C bond and the π-accepting property of the NHC ligand in achieving enhanced catalytic activity. Notably, catalyst activation occurred much more rapidly with the preformed palladium(0) complex compared to its palladium(II) counterpart.

Introduction

The development of efficient palladium complexes for catalyzing the Mizoroki–Heck coupling reaction of unreactive aryl halide substrates has garnered significant interest.[1–9] Various preformed palladium(II) complexes,[10] encompassing a wide range of ligand types such as cyclometallated ligands,[11] pincer ligands,[12] and electron-rich tertiary phosphines,[6,13] *etc.*, have been employed as pre-catalysts. Nevertheless, harnessing the potential of cost-effective aryl chlorides as substrates has been a challenging endeavor, largely due to the formidable strength of the C–Cl bonds. Over the past two decades, palladium complexes featuring *N*-heterocyclic carbene (NHC) ligands have emerged as highly versatile pre-catalysts for a wide array of cross-coupling reactions such as Suzuki–Miyaura, Sonogashira, Negishi, and Buchwald–Hartwig coupling reactions.[14–25] Some prominent examples of such palladium NHC complexes are shown in Scheme 1. Despite their extensive applicability, there remains a relative scarcity of literature regarding palladium NHC complexes capable of effectively activating C–Cl bonds in the Mizoroki–Heck coupling reaction, leading to a limited exploration of their potential in enabling the utilization of cost-effective aryl chlorides as substrates in this coupling

process.[26–29] The ligated zero-valent palladium complex is widely accepted as the active species in Pd-catalyzed transformations.[30–32] Consequently, preformed palladium(0) NHC complexes are anticipated to offer expedited catalyst activation compared to their palladium(II) NHC counterparts. Nevertheless, the literature on palladium(0) NHC complexes is still relatively limited.[33–40] As pre-catalysts, the preformed palladium(0) NHC complexes should exhibit ample stability for convenient handling and resist decomposition into palladium black when in solution.

Nitron, a mesoionic triazolium compound commercially known as 1,4-diphenyl-3-(phenylamino)-1*H*-1,2,4-triazolium inner salt, has been extensively utilized as an analytical compound for several decades.[41–44] Its tautomer form in solution assumes the form of a free NHC ligand which readily reacts with different transition metal precursors.[45–48] Previous studies have documented several palladium(II) NHC complexes derived from nitron (Scheme 2).[48,49] However, to our knowledge, there is no literature on their corresponding palladium(0) complexes incorporating nitron-based NHC ligands. In this study, we present new palladium(0) complexes with NHC ligands derived from nitron and its derivatives. Significantly, these new palladium(0) complexes exhibit excellent air stability and certain compounds exhibit exceptional efficiency in the Mizoroki–Heck coupling reaction, particularly when employing aryl chlorides as coupling partners. In-depth theoretical calculations have been performed to elucidate the electronic properties of these new ligands and their palladium(0) complexes, thereby providing insights into the design of effective precatalysts in the catalytic reaction.
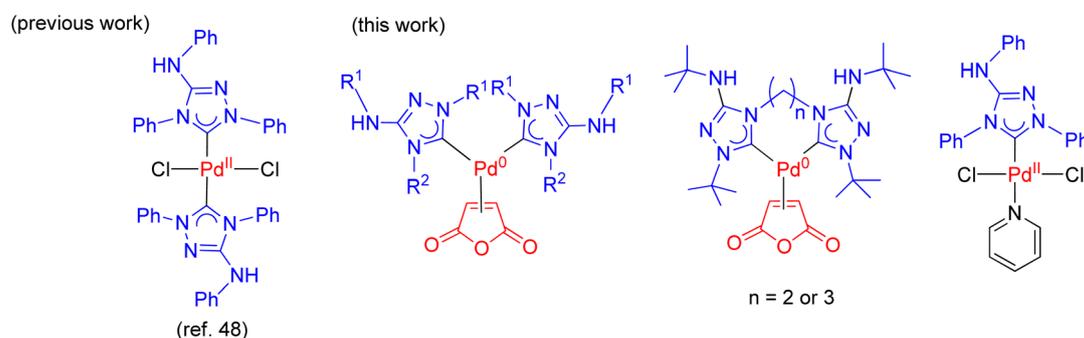
Department of Chemistry, National Changhua University of Education, Changhua 500, Taiwan. E-mail: leehm@cc.ncue.edu.tw
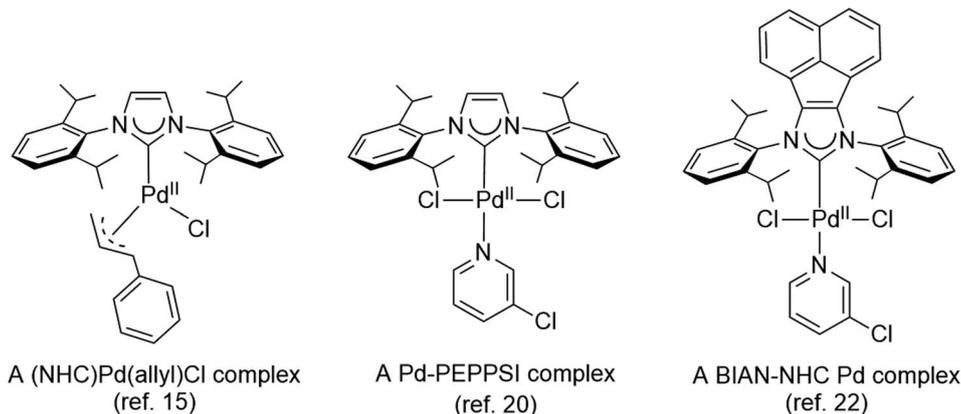
Scheme 1 Representative palladium NHC complexes as pre-catalysts in cross-coupling reactions.

Scheme 2 Palladium NHC complexes derived from nitron.

Results and discussion

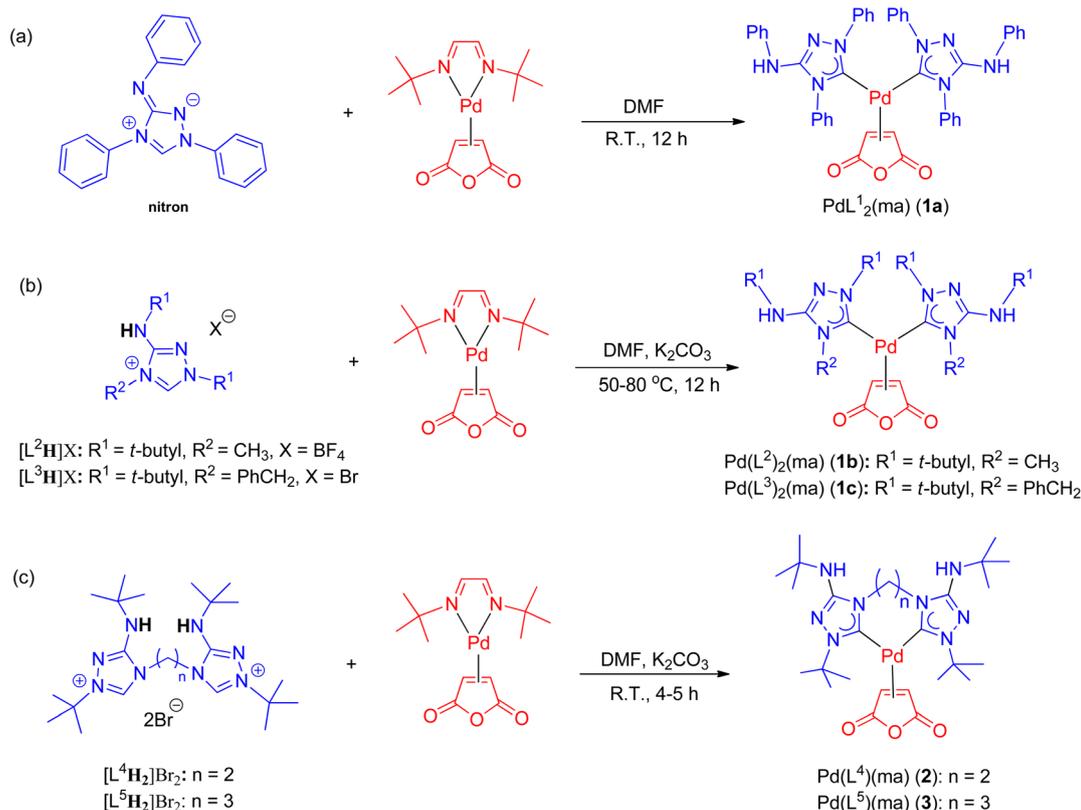### Synthesis of palladium(0) and palladium(II) NHC complexes

The synthesis of all new palladium complexes is depicted in Scheme 3. Nitron and other monodentate ligand precursors were obtained from commercial sources. To synthesize PdL$^1_2$(ma) (**1a**) (ma = maleic anhydride), the reaction between nitron and the palladium(0) precursor, Pd(dbd)(ma) (dbd = N,N'-ditert-butylethane-1,2-diimine),[50] was carried out in DMF at ambient temperature (Scheme 3a). In this particular reaction, the use of a base was unnecessary as the tautomer of nitron, which is the free carbene ligand L^1, was captured by Pd(dbd)(ma) in the solution. As a result, complex **1a** was obtained in a favorable yield of 90%. On the other hand, the synthesis of palladium(II) complex **4** involved the reaction between nitron and PdI$_2$ in neat pyridine, leading to the isolation of the pure product with a yield of 58% (Scheme 3d). In contrast, the preparation of PdL$^2_2$(ma) (**1b**) and PdL$^3_2$(ma) (**1c**) from triazolium precursors [L^{2}H]BF$_4$ and [L^{3}H]Br required the addition of potassium carbonate for the initial deprotonation of the acidic NH protons as depicted in Scheme 3b. Subsequently, tautomerizations occurred, resulting in the generation of free carbenes L^2 and L^3. Additionally, a higher temperature ranging from 50–80 °C was necessary for the formation of **1b** and **1c**, and the yields achieved were 84% and 66%, respectively.

The synthesis of palladium(0) complexes with bidentate carbene ligands followed a similar procedure as depicted in Scheme 3c. The ligand precursors [L^{4}H$_2$]Br$_2$ and [L^{5}H$_2$]Br$_2$, featuring bis(carbene) ligands with ethylene and propylene bridges (L^4 and L^5, respectively), were previously unknown. Detailed information regarding their preparation and characterization can be found in the ESI.† In the reactions involving Pd(dbd)(ma) and [L^{4}H$_2$]Br$_2$ or [L^{5}H$_2$]Br$_2$, K$_2$CO$_3$ was added as a base at room temperature. This resulted in the formation of palladium(0) complexes, namely PdL^4(ma) (**2**) and PdL^5(ma) (**3**), with moderate yields of 56% and 64%, respectively.

The successful formation of metal carbene complexes was confirmed by the presence of downfield carbene signals in their ^{13}C{^{1}H} NMR spectra. The carbene signals for the palladium monocarbene complexes **1a–c** were observed within a narrow range at 187.9, 184.6, and 185.6 ppm, respectively. Notably, complex **1a** with N-phenyl groups, exhibited a slightly more downfield carbene resonance compared to complexes **1b–c**, which had N-t-butyl groups. Interestingly, the carbene signal for palladium complex **3**, with propylene-linked carbene moieties, appeared at the typical chemical shift of 184.3 ppm, while the corresponding signal for palladium complex **2**, with ethylene-linked carbene ligands, showed an upfield shift at 177.9 ppm. This difference suggests the interplay of steric and electronic effects. In contrast, the carbene signal in palladium(II) complex
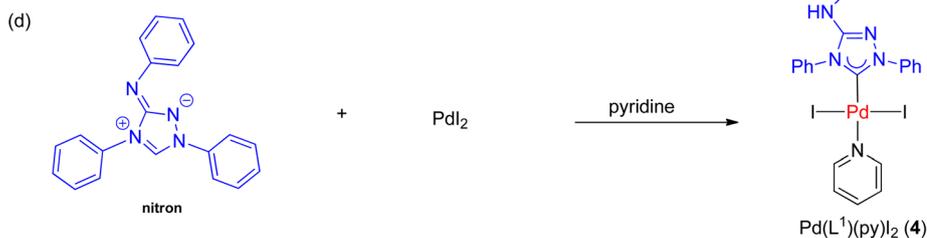
Scheme 3 Synthesis of palladium(0) NHC (a–c) and palladium(ii) NHC complexes (d).

4 appeared very upfield at 139.7 ppm compared to the palladium(0) complexes. Importantly, all the palladium(0) and palladium(ii) complexes were highly stable and could be easily handed in air.

Structural description

The structures of all new complexes, except **3**, were successfully determined through single-crystal diffraction studies (Fig. 1). The crystallographic data can be found in Table S1 in the ESI.† In an asymmetric unit, there were two independent molecules of **1c**, but only one of them was utilized for structural discussion. In each of the palladium(0) complexes, the coordination geometry around the metal center is formally trigonal planar, however, significant distortions were observed. For instance, in complex **1a**, the three angles between the Pd–carbene bonds and the centroid of C=C bond were measured to be 137.95°, 104.14°, 102.86°, deviating

substantially from the ideal 120°. The coordination geometry around the palladium(ii) center in complex **4** was a distorted square planar, with the two iodide ligands positioned in a *trans* configuration ($\angle$C–Pd–N = 174.4(2)°; $\angle$I–Pd–I = 175.59(2)°). Remarkably, the Pd–C bonds in palladium(0) complexes were much longer compared to the Pd–C bond in palladium(ii) complex **4** (**1a**: 2.073(3) and 2.038(3); **1b**: 2.074(5) and 2.088(5); **1c**: 2.087(5) and 2.109(5); **2**: 2.101(2) and 2.078(2) Å, while **4**: 1.954(5) Å). Additionally, a wide range of C–Pd–C angles was observed in the palladium(0) complexes. The angles in the complexes with monodentate NHC ligands (**1a**: 102.86(11)°; **1b**: 99.78(18)°; **1c**: and 111.13(19)°) were significantly smaller than the angle in the complex with the bidentate bis(NHC) ligand (**2**: 154.28(10)°).

Notable structural changes in the ligands upon metal coordination were observed. The C=C bond distances in the maleic anhydride ligands (**1a**: 1.437(4) Å; **1b**: 1.424(7) Å; **1c**: 1.447(8) Å;
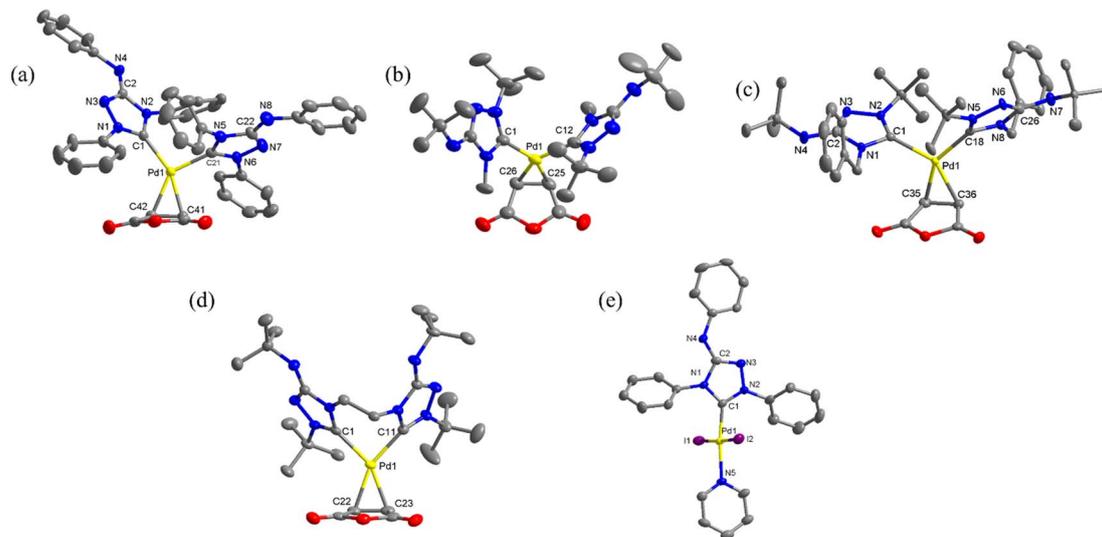
Fig. 1 The new molecular structures with thermal ellipsoids drawn at 50% probability level. Hydrogen atoms are omitted for clarity. (a) The molecular structure of **1a**; selected bond distances and angles (Å and °): Pd1–C1, 2.073(3); Pd1–C21, 2.038(3); Pd1–C41, 2.078(3); Pd1–C42, 2.162(3); C41–C42, 1.437(4); C1–Pd1–C21, 102.86(11); C1–Pd1–C42, 118.59(11); C21–Pd1–C41, 98.96(12); C1–Pd1–C41, 158.15(11); C21–Pd1–C42, 138.46(12). (b) The molecular structure of **1b**; selected bond distances and angles (Å and °): Pd1–C1, 2.074(5); Pd1–C12, 2.088(5); Pd1–C25, 2.090(5); Pd1–C26, 2.120(5); C25–C26, 1.424(7); C1–Pd1–C12, 99.78(18); C1–Pd1–C26, 113.8(2); C12–Pd1–C25, 106.77(19); C1–Pd1–C25, 153.3(2); C12–Pd1–C26, 146.20(19). (c) The molecular structure of **1c**; only one of the two independent molecules in an asymmetric unit is shown; selected bond distances and angles (Å and °): Pd1–C1, 2.087(5); Pd1–C18, 2.109(5); Pd1–C35, 2.098(5); Pd1–C36, 2.127(5); C35–C36, 1.447(8); C1–Pd1–C18, 111.13(19); C1–Pd1–C35, 99.8(2); C18–Pd1–C36, 108.7(2); C1–Pd1–C36, 139.8(2); C18–Pd1–C35, 148.4(2). (d) The molecular structure of **2**; selected bond distances and angles (Å and °): Pd1–C1, 2.101(2); Pd1–C11, 2.078(2); Pd1–C22, 2.113(2); Pd1–C23, 2.114(2); C22–C23, 1.444(4); C1–Pd1–C11, 89.59(9); C1–Pd1–C22, 114.37(9); C11–Pd1–C23, 116.04(10); C1–Pd1–C23, 154.28(10); C11–Pd1–C22, 155.96(10). (e) The molecular structure of **4**; selected bond distances and angles (Å and °): Pd1–C1, 1.954(5); Pd1–N5, 2.077(4); Pd1–I1, 2.6067(6); Pd–I2, 2.6000(6); C1–Pd1–I1, 88.91(16); C1–Pd1–I2, 88.11(17); N5–Pd1–I1, 92.97(13); N5–Pd1–I2, 90.30(13); C1–Pd1–N5, 174.4(2); I1–Pd1–I2, 175.59(2).

2: 1.444(4) Å) were found to be longer than the typical C=C bond length of 1.35 Å, indicating significant π-back bonding interactions between the d_π orbitals the Pd(0) centers and the π* orbitals of the C=C bonds. In all the palladium(0) complexes, the triazolium rings exhibited unsymmetrical bond lengths between the carbon and nitrogen atoms. Specifically, the NN–C bond was consistently shorter than the CN–C bonds by 0.23–0.53 Å. DFT calculations demonstrated that the shorter NN–C bonds possess a predominate double bond character

(*vide infra*). Interestingly, a linear correlation was observed between the Pd–C bond length and the CN–C distance (Fig. 2a). Complex **1a** exhibited the shortest CN–C bond and Pd–C bond among all the palladium(0) complexes, while complex **1c** displayed the longest bonds of both types. This correlation can be explained by the π electron density originating from the nitrogen atom of the CN–C bond, as well as the palladium(0) center, which donate into the vacant p-orbital of the carbenic carbon, resulting in shorter bonds.
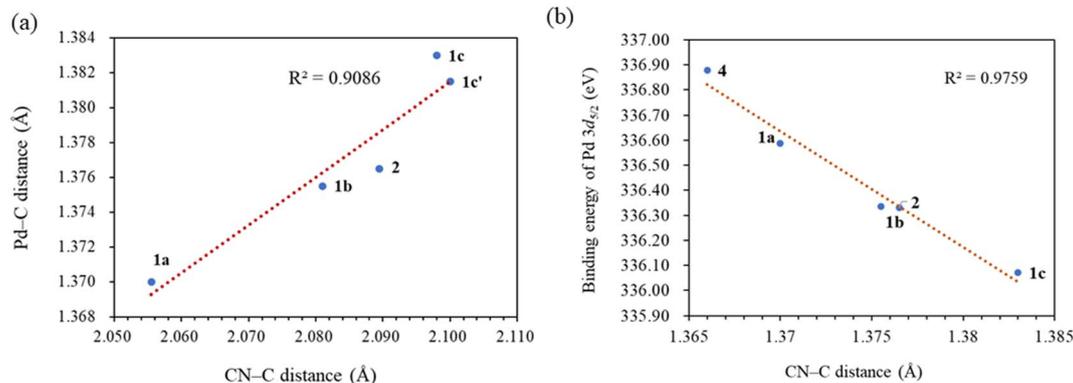

Fig. 2 (a) The correlation between Pd–carbene and CN–C distances in the X-ray structures. Complexes **1c** and **1c'** are the two independent molecules in an asymmetric unit. (b) The correlation between Pd $3d_{5/2}$ binding energies and CN–C distances.

Table 1 Electronic parameters of palladium complexes[a]

Complexes	3d$_{5/2}$ binding energy (eV)	WBIs of Pd–carbene bond
1a	336.59	0.5868[a]
1b	336.34	0.5655[a]
1c	336.07	0.5463[a]
2	336.33	0.5825[a]
3	336.28	0.5711[a]
4	336.88	0.6647

[a] There are two Pd–carbene bonds in the Pd(0) complexes. An average value is calculated.

X-ray photoelectron spectroscopy (XPS)

XPS spectra were utilized to investigate the electronic properties of the newly synthesized complexes, Table 1 presents the Pd 3d$_{5/2}$ binding energies of the complexes. Notably, Pd(II) complex **4** exhibited the highest binding energy of 336.88 eV, attributed to its higher nuclear charge, whereas all the other Pd(0) complexes have binding energies at least 0.29 eV lower. Among the Pd(0) complexes with monodentate NHC ligands, complex **1a**, featuring three *N*-phenyl substituents, displayed the highest binding energy, while complex **1c**, containing an electron-donating *N-tert*-butyl and *N*-benzyl groups, exhibited the lowest energy.

Interestingly, there exists a correlation between the increase in Pd 3d$_{5/2}$ binding energies and the decrease in CN–C bond distances in the heterocyclic rings ($R^2 = 0.9759$) (Fig. 2b). Subsequent computational studies supported these findings, revealing that ligand L^1 in complex **1a** possesses weaker σ-donating capabilities, resulting in a higher binding energy of the Pd 3d core levels. However, L^1 acts as a superior π-acceptor, reinforcing the coordination bond through π-backbonding, which leads to the shortest CN–C distance. Conversely, ligand L^3 in complex **1c** exhibits good σ-donating abilities but poor π-acceptor characteristics. Consequently, complex **1c** displays the lowest binding energy but the longest CN–C bond. This correlation demonstrates that the CN–C distance obtained from X-ray structural data serves as a convenient probe for determining the Pd 3d$_{5/2}$ binding energy.

Computational studies

DFT calculations were conducted using the Gaussian 09W program to gain more chemical insights into the new ligands and metal complexes.[51] Geometry optimizations and energy calculations for the free ligands were performed at the M06-2X/6-31g* level of theory. To account for the influence of the DMF solvent, the polarized continuum model (PCM) was employed.[52] The energies of carbene orbitals involved in metal coordination for the new monodentate carbene ligands are presented in Table 2. Among the three new carbene ligands, L^3 possesses the highest energy for the σ-donating orbital (−7.46 eV). This energy surpasses that of the commonly used IMes and IPr ligands. Conversely, L^1 is the least electron-donating carbene ligand, exhibiting the lowest energy for the σ-donating orbital (HOMO-2) at −8.09 eV. However, L^1 serves as an excellent π-acceptor due to its low-lying π-accepting orbital (LUMO) with an energy of only 0.18 eV. In contrast, the π-accepting orbitals in L^2 and L^3 possess significantly higher energies, indicating that these ligands primarily act as σ-donors.

Geometry optimizations for metal complexes were carried out using the B3LYP[53,54]/LANL2DZ[55] level of theory, based on the coordinates of the X-ray structural data. Energy calculations were performed using M06L functional with the def2-TZVP[56] basis set. The PCM was again employed to account for the solvent effect of DMF.[52] The Pd–C bond distances obtained from the X-ray structures and the optimized structures of the palladium complexes were compared, and the results are presented in Table 3. Overall, the optimized geometries closely agree with the experimental data. The Pd–C bond distances obtained from the optimized geometries are slightly larger, with deviations ranging from 0.008–0.046 Å. Notably, the computational

Table 2 σ-Donating and π-accepting orbitals in free carbene ligands and their calculated energies (M06-2X/6-31g*)
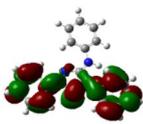
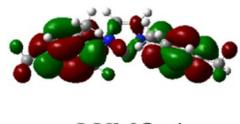| Ligand	L^1	L^2	L^3	IMes	IPr
π-accepting orbitals	LUMO (0.18 eV)	LUMO (2.34 eV)	LUMO+2 (2.26 eV)	LUMO+1 (0.81 eV)	LUMO+2 (0.80 eV)
σ-donating orbitals	HOMO−2 (−8.09 eV)	HOMO−1 (−7.56 eV)	HOMO−1 (−7.46 eV)	HOMO (−7.64 eV)	HOMO (−7.64 eV)
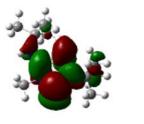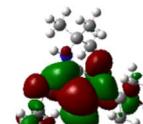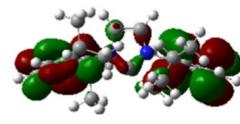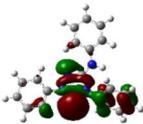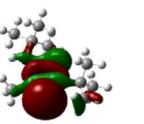
Table 3 Average Pd–C distances obtained from structural data and optimized structures[a]

Complexes	Pd–C distances from the X-ray data (Å)	Pd–C distances from the optimized structures (Å)	Difference between structural and computational data (Å)
1a[a]	2.056	2.092	−0.036
1b[a]	2.081	2.113	−0.032
1c[a]	2.100	2.131	−0.031
2[a]	2.090	2.098	−0.008
4	1.954	2.000	−0.046

[a] There are two Pd–C distances in the Pd(0) complexes. An average distance is calculated.

method demonstrates high accuracy in reproducing the X-ray data for the palladium complex **2**, which contains a bis(NHC) ligand, yielding a very small error of 0.008 Å. For palladium complexes with monodentate NHC ligands, a positive and linear relationship ($R^2 = 0.9999$) is observed between the experimental and computational Pd–C bond distances (Fig. 3a).

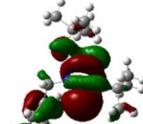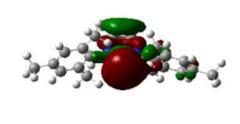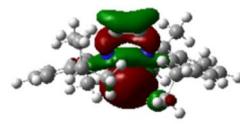The Frontier orbitals and their energies of palladium complexes **1a** and **4** are presented in Fig. 4. In complex **1a–c**, the HOMOs are distributed over the Pd atoms and carbene ligands, while the LUMOs are primarily localized on the coordinated maleic anhydride. This arrangement allows for facile nucleophilic attacks on the maleic anhydride moiety. In contrast, the HOMO of palladium(II) complex **4** is concentrated along the I–Pd–I axis, indicating a strong interaction between the iodine atoms and the palladium center. The LUMO, on the other hand, is found along both the I–Pd–I and C–Pd–N axes (Fig. 4).

The Wiberg bond indices (WBIs) were calculated using natural bond orbital (NBO) analysis[57] to determine the bond order between the palladium and carbene bonds. The average WBIs of the Pd–carbene bonds are presented in Table 1. The WBI of the well-known PEPPSI complex [trans-Pd(IPr)(3-Cl-py)Cl$_2$] was previously estimated to be 0.6871.[58] Notably, the Pd–carbene bonds in all the palladium(0) complexes are weaker compared to the Pd–carbene bond in the palladium(II) complex **4**, which is consistent with their bond distances observed in the structural studies (*vide supra*). Two factors contribute to these weaker bonds. Firstly, the maleic anhydride ligand is a strong π-acceptor, drawing electron density away from the palladium(0) centers. This significantly reduces the extent of π-backbonding

between the Pd(0) center and the NHC ligand. For instance, in complex **1a**, the C=C π* orbital in the maleic anhydride ligand is highly occupied (0.68751 electrons), indicating strong electron withdrawal. Secondly, the N–C bonds flanking the carbenic carbon are unequal in length. NBO analysis reveals that the shorter NN–C bonds possess significant double bond characters. For example, in complex **1a**, the average occupation of the σ and π bonding electrons between the C and N atoms are 1.98013 and 1.88249 electrons, respectively. Consequently, π-donation from the lone pair on the N atom of the longer CN–C bond to the substantially filled p$_\pi$ orbital on the carbenic carbon, as well as the π-backdonation from the Pd center, are significantly reduced. Consistently, there is an inverse correlation between the experimental Pd–carbene bond distances and the WBIs ($R^2 = 0.9979$), indicating that shorter bonds exhibit higher WBIs and *vice versa*. A positive correlation exists between Wiberg Bond Indices (WBIs) and Pd $3d_{5/2}$ binding energies within the trio palladium(0) complexes **1** with monodentate NHC ligands. Despite being a weaker σ-donating ligand, the carbene ligand in complex **1a** exhibits strong π-backbonding, resulting in its highest WBI (0.58675) and Pd $3d_{5/2}$ binding energy (336.59 eV) among the complexes. The CN–C bond distances from X-ray structures also align with WBIs; complex **1a**, having the highest WBI (0.58675), also features the shortest CN–C bond (1.370 A) among the trio.

The NBO second-order perturbation theory analysis provided average stabilizing energies of π-backdonation from the lone pairs of Pd atoms to the π* orbital of the C–N bonds. The values obtained were 8.49, 7.96, and 7.70 kcal mol^{-1} for complexes **1a**
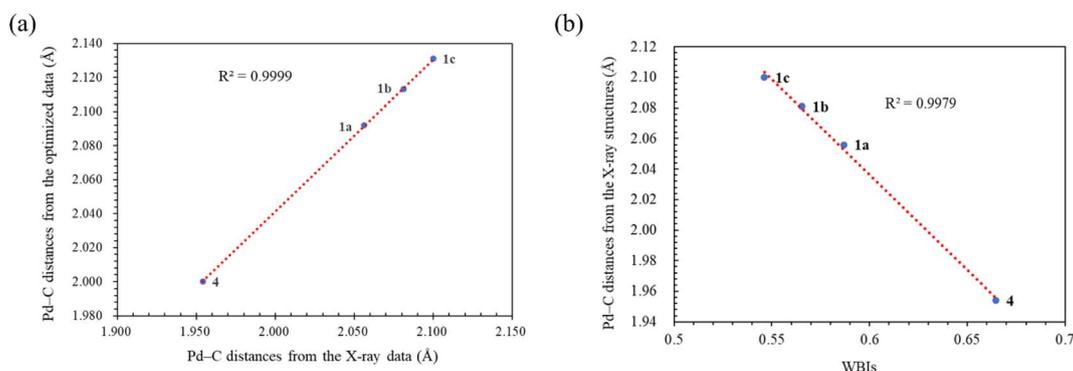

Fig. 3 (a) The linear correlation of the Pd–C distances between the X-ray and optimized structural data. (b) The correlation between Pd–C distances in the X-ray structures and WBIs.
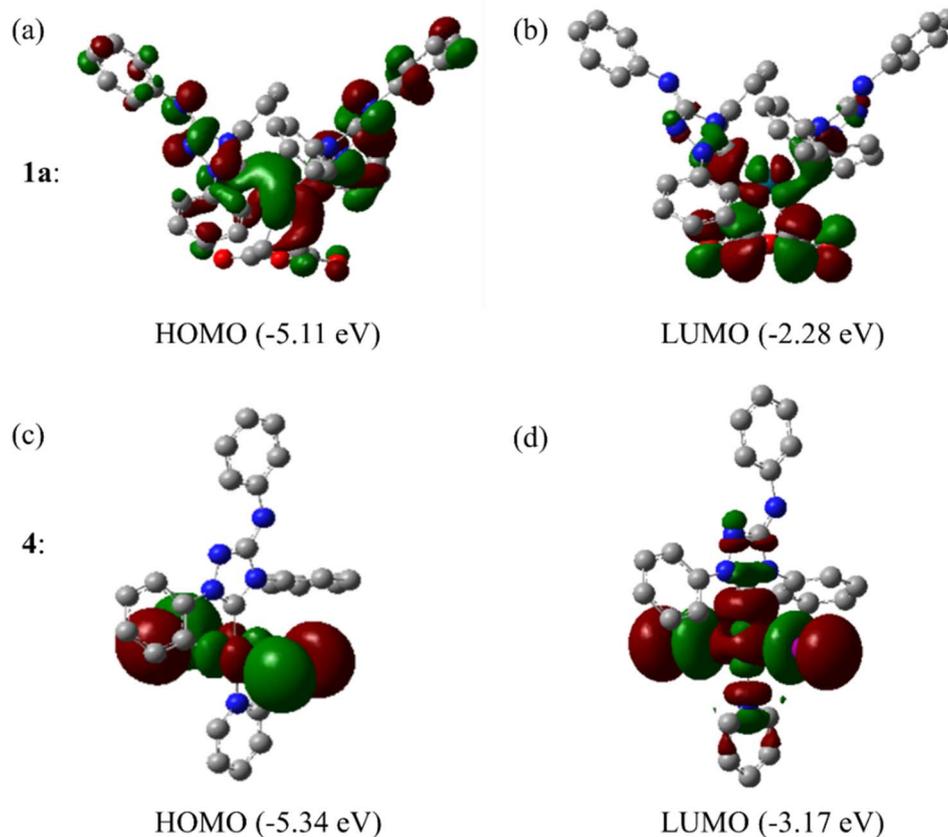
Fig. 4 Frontier orbitals in Pd(0) complex **1a** and Pd(II) complex **4**.

to **1c**, respectively. These values indicate the extent of π-back-donation from the Pd centers to the carbene ligands. To further confirm the different abilities of the new monodentate carbene ligands as π-acceptors in receiving backdonation from Pd centers, a charge decomposition analysis (CDA) was performed on LPd(0) (L = L^1, L^2, L^3).[59] The CDA results confirmed that L^1 is the most efficient π-acceptor, exhibiting the highest back-donation ratio (Table 4). Conversely, the extent of back-donation in L^2 and L^3 ligands was found to be similar. These CDA results are consistent with the π-accepting orbital energies of the ligands, as discussed earlier.

The analysis conducted in this part reveals important insights into the nature of the Pd–carbene bonds in the palladium(0) complexes. It is observed that these bonds are weaker compared to those found in Pd(II) complexes, primarily due to the presence of the strong π-accepting maleic

anhydride (MA) ligand in the palladium(0) complexes. Despite their weakened nature, significant backdonation from the Pd center to the carbene ligands is still observed, indicating the presence of a bonding interaction. Among the monodentate carbene ligands studied, L^1, which bears three *N*-phenyl rings, demonstrates the highest π-acceptor ability, while L^3, with three *N-tert*-butyl and one *N*-benzyl groups, exhibits the best σ-donor characteristics. The shorter NN–C bonds within the heterocyclic rings show significant double bond character, indicating a strong bonding interaction. Conversely, the longer CN–C bond distances in the carbene ligands correlate well with various electronic and structural parameters, including Pd 3d$_{5/2}$ binding energies, WBIs, and Pd–carbene bond distances. These findings provide valuable insights into the electronic and structural properties of the Pd–carbene bonds in the studied complexes, contributing to

Table 4 Charge decomposition analysis[a]

Complexes	d^b	b^c	r^d	$(d + b)$	$b/(d + b)$
L^{1}Pd	0.184444 (0.187785)	0.214079 (0.175547)	−0.228735 (−0.079429)	0.398523 (0.363332)	53.7% (48.3%)
L^{2}Pd	0.189166 (0.197697)	0.204760 (0.169322)	−0.241592 (−0.094406)	0.393926 (0.367019)	52.0% (46.1%)
L^{3}Pd	0.185302 (0.187185)	0.208898 (0.171341)	−0.223542 (−0.088492)	0.394200 (0.358526)	51.9% (47.8%)

[a] At the M06-L/def2TZVP level; at the PBE1PBE/def2-TZVP level in brackets. [b] Number of electrons donated from the ligand to the Pd atom. [c] Number of electrons donated from the Pd atom to the ligand. [d] Closed-shell interaction.

a better understanding of their reactivity and catalytic behavior.

Mizoroki–Heck coupling reaction

The newly synthesized palladium(0) complexes were evaluated as catalyst precursors in the Mizoroki–Heck coupling reaction. The coupling of 4-chloroacetophenone with styrene in neat tetrabutylammonium bromide (TBAB) was taken as the benchmark, following previously established conditions.[26,27] The catalyst screening results are summarized in Table 5. Remarkably, when a 0.2 mol% of Pd loading was employed, complex **1a**, which featured the monodentate L^1, as well as complexes **2** and **3**, containing bidentate bis(NHC) ligands L^4 and L^5, respectively, exhibited excellent yields of the coupling product (entries 1, 4, and 5). Interestingly, complexes **1b** and **1c**, which feature more electron-donating ligands L^2 and L^3, exhibited significantly lower effectiveness in the Mizoroki–Heck coupling reaction (entries 2 and 3). Typically, the rate-determining step (rds) involves the oxidative addition of the strong C–Cl bond in the aryl chloride to the Pd(0) species. Consequently, one would expect that the more electron-rich complexes **1b** and **1c** would exhibit higher activities compared to complex **1a**. However, experimental observations suggest that the actual rds might be different in the catalytic cycle, such as the reductive elimination. Furthermore, the stability of the palladium(0)–carbene bond might play a more crucial role in the catalytic reaction than solely the electron-rich nature of the complex itself. Complex **1a**, which possesses the strongest Pd–C bond among complexes **1a–c** due to enhanced π-back-bonding interactions (*vide supra*), was also compared to complex **2** featuring a bidentate bis(NHC) ligand. For this comparative study, the reaction time was shortened to 1 h. Remarkedly, complex **1a** demonstrated superior performance with a yield of 94%, while complex **2** yielded only 49% (entries 6 *vs.* 7). The time–yield curves of these two complexes are presented in Fig. S1 in the ESI.† It was determined that the optimized Pd loading for the reaction was 0.2 mol%, as reducing

the loading to 0.1 mol% resulted in a significant decrease in product yield to 17% (entry 8).

Following the identification of the most promising catalyst precursor **1a**, the substrate scope was further investigated (Table 6). The reaction time was partially optimized to achieve the best yields. Entries 1–6 clearly demonstrate that the catalyst system based on **1a** exhibited remarkable effectiveness in utilizing electron-deficient aryl chlorides in combination with styrene, resulting in isolated yields ranging from 62% to quantitative yield. The reactions were conducted at a temperature of 120 °C for 2 h. In contrast, the system exhibited lower efficiency when utilizing electron-neutral and electron-rich aryl chloride substrates, requiring a prolonged reaction time of 12 h to achieve reasonable yields of coupling products (entries 7 and 8). However, when electron-rich aryl bromide substrates were employed, excellent yields of the products were obtained. Notably, 97 and 99% product yields were achieved using 4-bromo- and 3-bromoanisole, respectively (entries 9 and 10). Furthermore, even sterically hindered 2-bromoanisole readily underwent coupling with styrene, yielding a 69% product yield (entry 11). The substituted 4-methoxystyrene was also tested as a substrate, and once again, activated aryl chloride substrates exhibited smooth reactivity, resulting in high product yields (entries 12–14). However, the coupling reaction with 4-chloroanisole showed a poor yield (entry 15). Additionally, the applicability of *n*-butylacrylate as a coupling partner was explored (entries 16–23). The reaction with 4-chloroacetophenone yielded a mediocre yield of 54% in 6 h (entry 16). Significantly improved results were obtained when the reaction was conducted at 140 °C, leading to an 81% yield of the coupling product in 2 h (entry 17). Electron-deficient aryl chlorides provided yields ranging from 40% to 96% (entries 18–21). However, the reactivity with electron-neutral or electron-rich aryl chloride substrates was less promising (entries 22 and 23).

Next, we compare the catalytic activities of palladium(0) complex **1a** with relevant Pd(II) NHC complexes (Table 7). A

Table 5 Screening of the new palladium(0) complexes for catalyzing the Mizoroki–Heck coupling reaction[a]
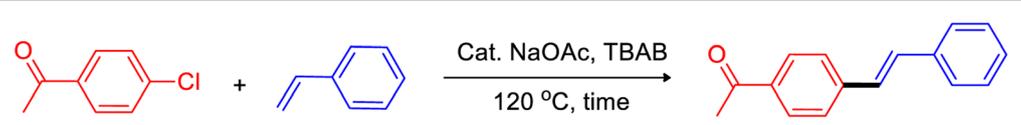
Entry	Cat	Pd mol%	Time (h)	Yield (%)	TON
1	**1a**	0.2	2	**98** (95 : 5)	490
2	**1b**	0.2	2	5	25
3	**1c**	0.2	2	54 (95 : 5)	270
4	**2**	0.2	2	98 (95 : 5)	490
5	**3**	0.2	2	97 (94 : 6)	485
6	**1a**	0.2	1	94 (95 : 5)	470
7	**2**	0.2	1	49 (95 : 5)	245
8	**1a**	0.1	1	17 (97 : 3)	170

[a] Reaction conditions: 1.4 mmol of styrene, 1 mmol of aryl halide, 1.1 mmol of NaOAc, 2 g of TBAB, Pd cat., 120 °C. Yield determined by using 1,3,5-trimethoxy-benzene as internal standard.

Table 6 Substrate scope[a]
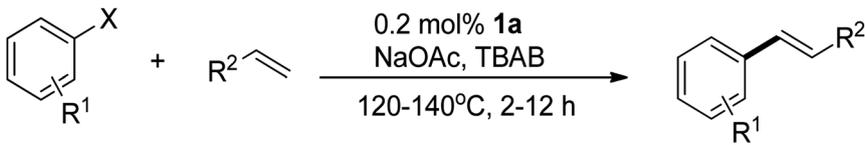
| entry	R^1	X	R^2	Product	Time	Yield (%)	TON
1	4-CH$_3$C(=O)	Cl	Ph	**5a**	2	99[b]	495
2	4-NO$_2$	Cl	Ph	**5b**	2	97[b]	485
3	4-C≡N	Cl	Ph	**5c**	2	76[b]	380
4	4-HC(=O)	Cl	Ph	**5d**	2	82[b]	410
5	4-CF$_3$	Cl	Ph	**5e**	2	72[b]	360
6	4-CH$_3$OC(=O)	Cl	Ph	**5f**	2	62[b]	310
7	H	Cl	Ph	**5g**	12	38	190
8	4-CH$_3$O	Cl	Ph	**5h**	12	52	260
9	4-CH$_3$O	Br	Ph	**5h**	12	97	485
10	3-CH$_3$O	Br	Ph	**5i**	12	99	495
11	2-CH$_3$O	Br	Ph	**5j**	12	69	345
12	4-CH$_3$C(=O)	Cl	4-CH$_3$OPh	**5k**	2	99, 90[b]	495, 490[b]
13	4-NO$_2$	Cl	4-CH$_3$OPh	**5l**	2	99	495
14	4-HC(=O)	Cl	4-CH$_3$OPh	**5m**	2	99	495
15	4-CH$_3$O	Cl	4-CH$_3$OPh	**5n**	12	17	85
16	4-CH$_3$C(=O)	Cl	CO$_2$^{n}Bu	**5o**	6	54[b]	270
17	4-CH$_3$C(=O)	Cl	CO$_2$^{n}Bu	**5o**	2	81	405
18	4-NO$_2$	Cl	CO$_2$^{n}Bu	**5p**	2	96	480
19	4-C≡N	Cl	CO$_2$^{n}Bu	**5q**	2	72	360
20	4-HC(=O)	Cl	CO$_2$^{n}Bu	**5r**	2	67	335
21	4-CF$_3$	Cl	CO$_2$^{n}Bu	**5s**	2	40	200
22	H	Cl	CO$_2$^{n}Bu	**5t**	12	11	55
23	4-CH$_3$O	Cl	CO$_2$^{n}Bu	**5u**	12	10	50

[a] Reaction conditions (unless otherwise specified): 1.0 mmol aryl halide, 1.4 mmol alkene, 1.1 mmol NaOAc, 2 g of TBAB, 0.2 mol% of **1a**, 140 °C unless specified otherwise., 2–12 h. Isolated yield. [b] 120 °C.

Table 7 Comparison of catalytic activities by different catalyst precursors[a]
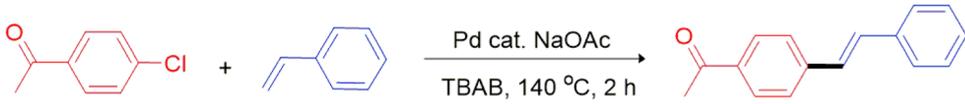
Entry	Pre-catalyst	Pd mol%	T (°C)	Time	Yield (%)	Reference
1	**1a**	0.2	140	2	99[b] (94 : 6)	This work
2	**4**	0.2	140	2	43[b] (93 : 7)	This work
3	Pd(OAc)$_2$	0.2	140	2	76[b] (97 : 3)	Ref. 27
4	Pd(IMes)Cl$_2$(3-Clpy)	0.2	140	2	26[b] (92 : 8)	Ref. 27
5	Tetranuclear Pd(aNHC)	0.2	140	2	>99[b] (95 : 5)	Ref. 27
6	Tetranuclear Pd(aNHC)	0.2	140	2	>99[b] (96 : 4)	Ref. 26
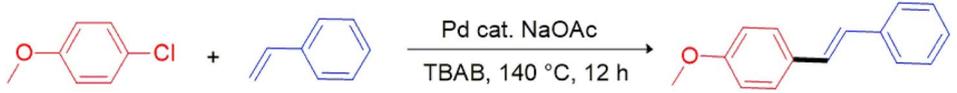
7	**1a**	0.2	140	12	52[c]	This work
8	Tetranuclear Pd(aNHC)	0.2	140	12	64[c]	Ref. 27
9	Tetranuclear Pd(aNHC)	0.2	140	12	>99[c]	Ref. 26

[a] Reaction conditions: 1.4 mmol of styrene, 1 mmol of aryl halide, 1.1 mmol of NaOAc, 2 g of TBAB, monopalladium loading, 140 °C. [b] Yield determined by using 1,3,5-trimethoxy-benzene as internal standard. [c] Isolated yield.
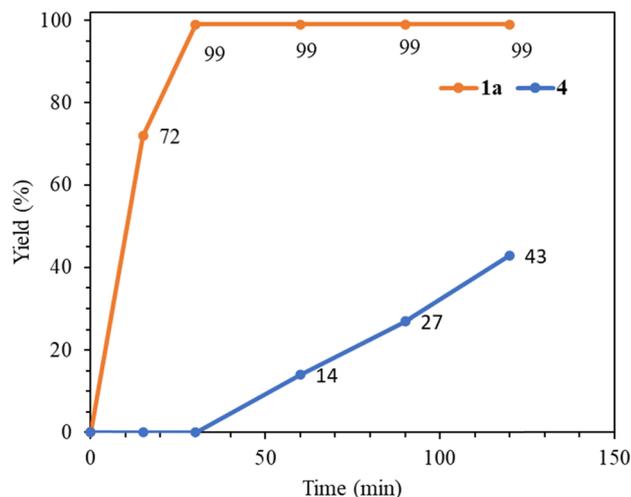
Fig. 5 Time-yield curves of complexes **1a** and **4** in the catalytic reaction between 4-chloroacetophenone and styrene carried out at 140 °C.

comparison of entries 1 and 2 clearly indicates that the palladium(0) complex **1a** functions as a significantly better precatalyst than the palladium(II) complex **4**. The time–yield curves for **1a** and **4** in the benchmark reaction are presented in Fig. 5, highlighting that complex **4** requires an activation time of 30 min to transform into an active Pd(0) species, while complex **1a** essentially completes the reaction within that time frame. Additionally, complex **1a** demonstrates superior catalytic activity compared to simple Pd(OAc)$_2$ and the PEPPSI complex, *trans*-Pd(IPr)(3-Cl-py)Cl$_2$ (entries 1 *versus* 3 and 4). Tetranuclear palladium(II) complexes with abnormal NHC ligands have exhibited high activity in the Mizoroki–Heck coupling reaction.[27] Furthermore, the activity of **1a** is comparable to multinuclear catalyst systems when utilizing the electron-poor 4-chloroacetophenone substrate (entries 1 *versus* 5 and 6). However, it exhibits lower efficiency in the utilization of unreactive 4-chloroanisole compared to the tetranuclear catalyst systems (entries 7 *versus* 8 and 9).

In order to determine the nature of the catalytic species involved in the reaction, a Hg drop test was performed. Excess Hg (Hg : Pd = 100 : 1) was added to the benchmark reaction, and a slightly lower yield of 74% was obtained compared to the original reaction. This result suggests that the major catalytic species in the reaction is likely to be homogeneous, indicating that the palladium complex is predominantly responsible for the observed catalytic activity. In the Mizoroki–Heck reaction, the C–Cl bond in an aryl chloride undergoes oxidative addition to Pd(0) to form a Pd(II) intermediate.[32] To confirm the presence of this Pd(II) species in the catalytic cycle, a solution of Pd(0) complex **1a** and 4-chloroacetophenone in a 1 : 1 ratio in DMF was heated to 140 °C for 2 h. After the reaction, the solution was removed, and XPS analysis of the solid remained revealed a 3d$_{5/2}$ binding energy of 336.868 eV for the Pd residue. This value closely resembles the 3d$_{5/2}$ binding energy of the Pd(II) complex **4** (336.878 eV), indicating a change in valency from 0 to +2 and supporting the conversion of Pd(0) to Pd(II) species in the catalytic cycle.

Conclusions

The synthesis of stable palladium(0) complexes with monodentate and bis(carbene) ligands based on nitron and its derivatives was successfully achieved. The Pd–carbene bonds in these complexes are weaker compared to Pd(II) complexes due to the presence of strong π-accepting maleic anhydride (MA) ligands. However, significant back-donation still occurs, with the best π-acceptor being L^1 with three *N*-phenyl rings, and the best σ-donor being L^3 with three *N-tert*-butyl and one *N*-benzyl groups.

The shorter NN–C bonds in the heterocyclic rings exhibit double bond character, while longer CN–C bond distances correlate with various electronic and structural parameters, such as Pd 3d$_{5/2}$ binding energies, Wiberg bond indices (WBIs), and Pd–carbene bond distances.

Among the complexes, **1a** with monodentate ligand L^1 and a strong Pd–C bond, attributed to enhanced π-back-bonding, was identified as the best catalyst precursor for the Mizoroki–Heck coupling reaction between alkenes and aryl chloride substrates. The catalytic system showed excellent performance with activated aryl chloride substrates, yielding high coupling product yields. However, complexes **1b** and **1c** with more electron-donating ligands (L^2 and L^3) were found to be less effective, emphasizing the importance of the stability of the palladium(0) precatalyst over the electron-richness of the complex in the catalytic reaction which necessitate a high heating temperature. In comparison, palladium(0) complex **1a** outperformed palladium(II) complex **4**, with a significantly shorter activation time required for complex **1a** to generate an active species. This study highlights the significance of a strong metal–carbene bond, crucial for palladium complexes to serve as efficient precatalysts in the Mizoroki–Heck coupling reaction.

Conflicts of interest

No competing financial interests are declared by the authors.

Acknowledgements

References

1 M. Portnoy, Y. Ben-David, I. Rousso and D. Milstein, *Organometallics*, 1994, **13**, 3465–3479.
2 W. A. Herrmann, C. Brossmer, C.-P. Reisinger, T. H. Riermeier, K. Öfele and M. Beller, *Chem. - Eur. J.*, 1997, **3**, 1357–1364.
3 M. T. Reetz, G. Lohmer and R. Schwickardi, *Angew Chem Int. Ed.*, 1998, **37**, 481–483.
4 M. Beller and A. Zapf, *Synlett*, 1998, **1998**, 792–793.
5 A. F. Littke and G. C. Fu, *J. Org. Chem.*, 1999, **64**, 10–11.
6 A. F. Littke and G. C. Fu, *Angew Chem Int. Ed.*, 2002, **41**, 4176–4211.

7 R. B. Bedford, C. S. J. Cazin and D. Holder, *Coord. Chem. Rev.*, 2004, **248**, 2283–2321.

8 A. Zapf and M. Beller, *Chem. Commun.*, 2005, 431–440.

9 K. R. Balinge and P. R. Bhagat, *C. R. Chim.*, 2017, **20**, 773–804.

10 H. Li, C. C. C. Johansson Seechurn and T. J. Colacot, *ACS Catal.*, 2012, **2**, 1147–1164.

11 V. K. Jain, *Coord. Chem. Rev.*, 2021, **427**, 213546.

12 L. González-Sebastián and D. Morales-Morales, *J. Organomet. Chem.*, 2019, **893**, 39–51.

13 C. A. Fleckenstein and H. Plenio, *Chem. Soc. Rev.*, 2010, **39**, 694–711.

14 W. A. Herrmann, K. Öfele, D. v. Preysing and S. K. Schneider, *J. Organomet. Chem.*, 2003, **687**, 229–248.

15 N. Marion, O. Navarro, J. Mei, E. D. Stevens, N. M. Scott and S. P. Nolan, *J. Am. Chem. Soc.*, 2006, **128**, 4101–4111.

16 E. A. B. Kantchev, C. J. O'Brien and M. G. Organ, *Angew Chem Int. Ed.*, 2007, **46**, 2768–2813.

17 N. Marion and S. P. Nolan, *Acc. Chem. Res.*, 2008, **41**, 1440–1449.

18 S. Díez-González, N. Marion and S. P. Nolan, *Chem. Rev.*, 2009, **109**, 3612–3676.

19 G. C. Fortman and S. P. Nolan, *Chem. Soc. Rev.*, 2011, **40**, 5151–5169.

20 C. Valente, S. Çalimsiz, K. H. Hoi, D. Mallik, M. Sayah and M. G. Organ, *Angew Chem Int. Ed.*, 2012, **51**, 3314–3332.

21 M. N. Hopkinson, C. Richter, M. Schedler and F. Glorius, *Nature*, 2014, **510**, 485–496.

22 C. Chen, F.-S. Liu and M. Szostak, *Chem. - Eur. J.*, 2021, **27**, 4478–4499.

23 J. Li, D. He, Z. Lin, W. Wu and H. Jiang, *Org. Chem. Front.*, 2021, **8**, 3502–3524.

24 S. J. Firsan, V. Sivakumar and T. J. Colacot, *Chem. Rev.*, 2022, **122**, 16983–17027.

25 G. R. Peddiahgari Vasu, K. R. Motakatla Venkata, R. R. Kakarla, K. V. S. Ranganath and T. M. Aminabhavi, *Environ. Res.*, 2023, **225**, 115515.

26 J.-Y. Lee, Y.-S. Su, Y.-S. Wang and H. M. Lee, *Adv. Synth. Catal.*, 2019, **361**, 4714–4726.

27 C.-H. Hung, W.-Y. Zheng and H. M. Lee, *Organometallics*, 2021, **40**, 702–713.

28 P. J. Anju, M. Neetha and G. Anilkumar, *ChemistrySelect*, 2022, 7, e202103564.

29 Z. Zeng, Y. Chen, X. Zhu and L. Yu, *Chin. Chem. Lett.*, 2023, **34**, 107728.

30 C. Amatore and A. Jutand, *Acc. Chem. Res.*, 2000, **33**, 314–321.

31 J. P. Knowles and A. Whiting, *Org. Biomol. Chem.*, 2007, **5**, 31–44.

32 C. S. Wei, G. H. M. Davies, O. Soltani, J. Albrecht, Q. Gao, C. Pathirana, Y. Hsiao, S. Tummala and M. D. Eastgate, *Angew Chem Int. Ed.*, 2013, **52**, 5822–5826.

33 V. P. W. Böhm, C. W. K. Gstöttmayr, T. Weskamp and W. A. Herrmann, *J. Organomet. Chem.*, 2000, **595**, 186–190.

34 N. D. Clement, K. J. Cavell and L.-l. Ooi, *Organometallics*, 2006, **25**, 4155–4165.

35 S. Fantasia and S. P. Nolan, *Chem. - Eur. J.*, 2008, **14**, 6987–6993.

36 J.-Y. Lee, P.-Y. Cheng, Y.-H. Tsai, G.-R. Lin, S.-P. Liu, M.-H. Sie and H. M. Lee, *Organometallics*, 2010, **29**, 3901–3911.

37 S. N. Sluijter, S. Warsink, M. Lutz and C. J. Elsevier, *Dalton Trans.*, 2013, **42**, 7365–7372.

38 Y.-M. Jhou, D. Nandi, J.-Y. Lee, R.-J. Tzeng and H. M. Lee, *Polyhedron*, 2015, **100**, 28–35.

39 T. Scattolin, C. Santo, N. Demitri, L. Canovese and F. Visentin, *Dalton Trans.*, 2020, **49**, 5684–5694.

40 A. F. Henwood, M. Lesieur, A. K. Bansal, V. Lemaur, D. Beljonne, D. G. Thompson, D. Graham, A. M. Z. Slawin, I. D. W. Samuel, C. S. J. Cazin and E. Zysman-Colman, *Chem. Sci.*, 2015, **6**, 3248–3261.

41 W. C. Cope and J. Barab, *J. Am. Chem. Soc.*, 1917, **39**, 504–514.

42 R. C. Young and P. M. Hernays, *Ind. Eng. Chem., Anal. Ed.*, 1940, **12**, 90.

43 M. Bobtelsky and J. Eisenstaedter, *Anal. Chim. Acta*, 1959, **20**, 216–227.

44 A. Hulanicki and M. Maj, *Talanta*, 1975, **22**, 767–769.

45 C. Färber, M. Leibold, C. Bruhn, M. Maurer and U. Siemeling, *Chem. Commun.*, 2012, **48**, 227–229.

46 S. Hitzel, C. Färber, C. Bruhn and U. Siemeling, *Organometallics*, 2014, **33**, 425–428.

47 C. Thie, S. Hitzel, L. Wallbaum, C. Bruhn and U. Siemeling, *J. Organomet. Chem.*, 2016, **821**, 112–121.

48 P. J. Quinlivan, A. Loo, D. G. Shlian, J. Martinez and G. Parkin, *Organometallics*, 2021, **40**, 166–183.

49 A. Y. Chernenko, A. V. Astakhov, V. V. Kutyrev, E. G. Gordeev, J. V. Burykina, M. E. Minyaev, V. N. Khrustalev, V. M. Chernyshev and V. P. Ananikov, *Inorg. Chem. Front.*, 2021, **8**, 3382–3401.

50 K. J. Cavell, D. J. Stufkens and K. Vrieze, *Inorg. Chim. Acta*, 1981, **47**, 67–76.

51 M. J. Frisch, G. W. Trucks, H. B. Schlegel, G. E. Scuseria, M. A. Robb, J. R. Cheeseman, G. Scalmani, V. Barone, B. Mennucci, G. A. Petersson, H. Nakatsuji, M. Caricato, X. Li, H. P. Hratchian, A. F. Izmaylov, J. Bloino, G. Zheng, J. L. Sonnenberg, M. Hada, M. Ehara, K. Toyota, R. Fukuda, J. Hasegawa, M. Ishida, T. Nakajima, Y. Honda, O. Kitao, H. Nakai, T. Vreven, J. A. Montgomery Jr, J. E. Peralta, F. Ogliaro, M. Bearpark, J. J. Heyd, E. Brothers, K. N. Kudin, V. N. Staroverov, R. Kobayashi, J. Normand, K. Raghavachari, A. Rendell, J. C. Burant, S. S. Iyengar, J. Tomasi, M. Cossi, N. Rega, J. M. Millam, M. Klene, J. E. Knox, J. B. Cross, V. Bakken, C. Adamo, J. Jaramillo, R. Gomperts, R. E. Stratmann, O. Yazyev, A. J. Austin, R. Cammi, C. Pomelli, J. W. Ochterski, R. L. Martin, K. Morokuma, V. G. Zakrzewski, G. A. Voth, P. Salvador, J. J. Dannenberg, S. Dapprich, A. D. Daniels, Ö. Farkas, J. B. Foresman, J. V. Ortiz, J. Cioslowski and D. J. Fox, *Gaussian 09 (Revision D.01)*, Gaussian, Inc., Wallingford CT, 2009.

52 V. Barone and M. Cossi, *J. Phys. Chem. A*, 1998, **102**, 1995–2001.

53 A. D. Becke, *Phys. Rev. A*, 1988, **38**, 3098–3100.

54 C. Lee, W. Yang and R. G. Parr, *Phys. Rev. B*, 1988, **37**, 785–789.

55 T. H. Dunning Jr and P. J. Hay, in *Modern Theoretical Chemistry*, ed. H. F. Schaefer III, Plenum, New York, 1977, vol. 3, pp. 1–28.

56 F. Weigend and R. Ahlrichs, *Phys. Chem. Chem. Phys.*, 2005, **7**, 3297–3305.

57 E. D. Glendening, A. E. Reed, J. E. Carpenter and F. Weinhold, *NBO Version 3.1, TCI*, University of Wisconsin, Madison, 1998.

58 M. M. Rahman, J. Zhang, Q. Zhao, J. Feliciano, E. Bisz, B. Dziuk, R. Lalancette, R. Szostak and M. Szostak, *Organometallics*, 2022, **41**, 2281–2290.

59 S. Dapprich and G. Frenking, *J. Phys. Chem.*, 1995, **99**, 9352–9362.